The Astrophysical Journal, 646:76–84, 2006 July 20

O VI ASYMMETRY AND AN ACCELERATED OUTFLOW IN AN OBSCURED SEYFERT: *FUSE* AND *HST* STIS SPECTROSCOPY OF MRK 533

Prajval Shastri
Indian Institute of Astrophysics, Sarjapur Road, Bangalore 560034, India; pshastri@iiap.res.in

John Hutchings
National Research Council, Herzberg Institute of Astrophysics, 5071 West Saanich Road, Victoria, BC V9E 2E7, Canada

Jayant Murthy
Indian Institute of Astrophysics, Sarjapur Road, Bangalore 560034, India

Mark Whittle
Department of Astronomy, University of Virginia, Charlottesville, VA 22903

and

Beverley J. Wills
Department of Astronomy, University of Texas, 1 University Station, C1400, Austin, TX 78712
Received 2005 April 7; accepted 2006 March 28

ABSTRACT

We present far-ultraviolet spectra of the Seyfert 2 galaxy Mrk 533 obtained with *FUSE*. These spectra show narrow asymmetrical O VI $\lambda\lambda$1032,1038 emission lines with stronger wings shortward of the peak wavelength, but the degree of asymmetry of these wings in velocity is much lower than that of the wings of the lines of lower ionization. In the combined O VI profile there are marginal indications of local absorptions in the outflow. The C III λ977 line is seen weakly with a similar profile, but with very low signal-to-noise ratio (S/N). These FUV spectra are among the first for a Seyfert of type 2, i.e., a purportedly obscured Seyfert. The *HST* STIS spectral image of Mrk 533 allows delineation of the various components of the outflow, and we infer that the outflow is accelerated. We discuss the results in terms of nuclear geometry and kinematics.

Subject headings: galaxies: active — galaxies: individual (NGC 7674, Mrk 533)

1. INTRODUCTION

Seyfert galaxies have been long recognized as a class of active galactic nuclei (AGNs) that occupies the low end of the AGN luminosity range. They are primarily characterized by strong optical emission lines with implied Doppler broadening $\lesssim$300 km s^{-1} and a wide range of ionization (e.g., Osterbrock 1989). They are also characterized by strong X-ray emission (e.g., Elvis et al. 1978). In addition, Seyferts are usually radio-quiet, are in spiral host galaxies, and have central luminosities below the commonly adopted limit for quasars of $M_B^{\rm total} = -23$ (e.g., Schmidt & Green 1983).

Seyferts have traditionally been classified into types 1 and 2, distinguished primarily by the clear presence or absence of a component to the permitted lines in their spectra that is significantly broader than their forbidden lines. The Unified Scheme (e.g., Antonucci 1993) attempts to unify the two Seyfert types by hypothesizing a ubiquitous obscuring torus around their nuclei; the central emission (including the broad permitted line component) is then obscured when the Seyfert is oriented with its torus edge-on, and it appears to us as a Seyfert 2. When the torus is pole-on, the broad emission lines from the central clouds are directly visible, and the Seyfert is classified as type 1. The Unified Scheme found particularly strong support in the discovery of weak polarized broad lines from Seyfert 2 galaxies (Antonucci & Miller 1985; Moran et al. 2000), which are interpreted as originating from the hidden clouds but scattered periscopically into our line of sight.

The Unified Scheme is conceptually appealing, and many observational results are consistent with its predictions, including (1) the detection in Seyfert 2 galaxies of broad lines of Paβ, to which the torus is expected to be transparent (Veilleux et al. 1997); (2) the paucity of measured ionizing photons in Seyfert 2 galaxies, consistent with the torus attenuating the ionizing continuum emitted along our line of sight (e.g., Kinney et al. 1991); (3) the "double-cone" morphology of the narrow emission-line structures, interpreted as due to the torus shadowing the central ionizing photons (Schmitt et al. 2003; Ruiz et al. 2005); and (4) the similarity of the circumnuclear environments (Pogge & Martini 2002) and the luminosities of the molecular gas in Seyfert 1 and 2 galaxies (Curran et al. 2001). The universal validity of the Unified Scheme is still open to debate, however, with some results inconsistent with it, including (1) Seyfert 1 host galaxies being of earlier Hubble type than Seyfert 2 galaxies (Malkan et al. 1998), and (2) the galaxy densities around Seyfert 1 and 2 galaxies being dissimilar (Dultzin-Hacyan et al. 1999).

In the context of the Unified Scheme, we aim to compare the hot gaseous outflows in Seyferts of the purportedly pole-on and edge-on kinds, as manifested in the O VI $\lambda\lambda$1032, 1038 emission-line doublet along with any absorption that might be associated with it. This is possible using *FUSE* (*Far Ultraviolet Spectroscopic Explorer*; Moos et al. 2000; Sahnow et al. 2000), which can observe these wavelengths with spectral resolution $\lambda/\Delta\lambda$ of up to $\sim$20,000. In the framework of unification, we can interpret any similarities and differences in terms of the geometry and viewing angle.

Here we present the results from our first observations, which were of Mrk 533 (NGC 7674), a Seyfert 2 at a redshift of 0.0289. It is the brightest galaxy in the gravitationally interacting compact group Hickson 96 (Verdes-Montenegro et al. 1997) and has

its host galaxy oriented close to face-on with the ratio of major to minor axes of ~0.91 (de Vaucouleurs et al. 1995 [RC3]). Mrk 533 has radio jets on the 100 pc scale (Momjian et al. 2003). Spectropolarimetric observations (Miller & Goodrich 1990; Tran 1995) have revealed a broad (FWHM ~ 2830 km s^{-1}) Hβ line in polarized light, suggesting the presence of a genuine broad-line region hidden by obscuring material in our line of sight. Mrk 533 has its optical continuum polarized (probably due to dust scattering) at a position angle (P.A.) perpendicular to its radio axis (Tran 1995). It also shows evidence for Compton-thick X-ray emission and a reflection-dominated hard X-ray spectrum (Malaguti et al. 1998). Further, it shows H I absorption in the nuclear region (Beswick et al. 2002) and has long been known to have a spectacular blue wing to its [O III] λ5007 profile (e.g., Afanasev et al. 1980; Unger et al. 1988). The physical conditions of its narrow-line region were modeled from optical and *International Ultraviolet Explorer* (*IUE*) spectra by Kraemer et al. (1994).

We assume a Hubble constant of 75 km s^{-1} Mpc^{-1}, which gives a scale of 541 pc arcsec^{-1}.

2. THE OBSERVATIONS AND DATA REDUCTIONS

Mrk 533 was observed with the twin Rowland circle spectrographs on *FUSE* during two separate pointings, on 2002 August 18 for 10,478 s and on 2002 August 20 for 10,851 s. The spectra were taken through the largest aperture, which has a size $30'' \times 30''$ (the "LWRS"). The ultraviolet photons are detected on microchannel plate detectors, simultaneously via four independent optical channels, each of bandwidth ~200 Å. Two of these channels use Al+LiF coatings on the optics, and the other two use SiC coatings (cf. Sahnow et al. 2000). The Mrk 533 data were recorded in a total of 10 exposures, in photon-counting "time-tag" mode. Due to astigmatic effects on the spectra, no reliable spatial information in the cross-dispersion direction can be obtained. The final spectral resolution is primarily constrained by the drifts of the object within the aperture. Only one of the channels, viz., the LiF1A, is continuously aligned on target by the guiding camera (the Fine Error Sensor), whereas the alignment with the rest of the channels is done on orbital timescales.

Mrk 533 was also observed by the *Hubble Space Telescope* (*HST*) Space Telescope Imaging Spectrograph (STIS) on 2000 September 12. The $52'' \times 0\farcs2$ slit was centered on the peak of the stellar continuum and oriented at a P.A. of 124°, chosen to lie close to the two slightly different radio axes seen in the 15 GHz image of Unger et al. (1988). We present data obtained with an 1140 s exposure using the G430M grating, which gives a coverage of 280 Å centered on a wavelength of 5095 Å and sampled at 0.276 Å pixel^{-1} (FWHM = 2.5 pixels). The spatial scale is $0\farcs05$ pixel^{-1}.

2.1. *The Pipelined Data from FUSE*

Preprocessed data from the *FUSE* pipeline (CalFUSE ver. 3.1.0)[1] were used for this work. This pipeline processing included (1) removing the effects of the thermally induced drifts of the target image on the detector via modeling, (2) flat fielding using the prelaunch two-dimensional flat field and the one-dimensional on-orbit flat field obtained by observing FUV-bright dwarfs, (3) conversion of wavelengths to the heliocentric reference frame and their calibration, and (4) averaging the two-dimensional spectral image in the cross-dispersion direction to give a one-dimensional spectrum.

The relative motion of the spectrum on the detectors on an orbital timescale results in shifting of the zero point of the wavelength scale on the detector. From interstellar features, we found that these changes were $\leq$0.15 Å, which at the observed wavelength of the O VI line corresponds to $\leq$45 km s^{-1}.

2.2. *The Co-added FUSE Spectrum*

Data from all 10 exposures in each of the channels were co-added. Because of their low effective area and the low signal, the data from the SiC channels were not usable, and therefore we only used data from the LiF1 and LiF2 channels. Their effective area amounts to ~26 cm^2. Photons from each of these channels are imaged by the optics onto two segments of the detector, labeled A and B. Thus, the LiF1A and LiF2B data have overlapping coverage of the ~1000–1090 Å region, and the LiF2A and LiF1B data both cover the ~1090–1190 Å region. A comparison of the count rates with time in the LiF2 indicates that relative to the LiF1 channel there is no significant systematic loss of signal in it, and therefore no significant misalignment of the channels has occurred during the exposures. The signal in the two LiF channels is comparable, and they were combined to form a single mean spectrum.

The co-added data were averaged along the cross-dispersion direction to obtain a one-dimensional spectrum. The pixels were binned along the dispersion direction by a factor of 8 to ~0.05 Å per bin.

2.3. *Derivation of the FUSE Background*

The *FUSE* background is due to intrinsic detector background, the detector environment, and scattered light. We did not use the background subtraction from the CalFUSE pipeline, since the pipeline extractions gave negative flux values for our data, which indicates oversubtraction of the background. Instead, we used an empirical subtraction procedure of Murthy & Sahnow (2004) that uses the neighborhood pixels next to the spectrum.

The procedure assumes that the value of the instrumental background within the aperture is identical to the value just off the aperture. The raw *FUSE* data were processed through the CalFUSE pipeline with the background subtraction turned off. The resultant co-added two-dimensional data from each of the two exposures were then used. Data on either side of the desired aperture were averaged in the cross-dispersion direction and smoothed by a box average in the dispersion direction to obtain the background spectrum. Although this procedure results in some smoothing of any wavelength dependence of the background, it is clearly more representative and moreover gives flux values that lie above zero. We note that the spectral dependence of the background does not vary between orbital day and orbital night. Therefore, the subtraction was done without separating the orbital day and night data. Further, within the noise, the background-subtracted data are consistent between the two different *FUSE* exposures, and also between the two LiF detectors with overlapping wavelength coverage, which vindicates our procedure.

2.4. *Contamination of the FUSE Spectrum by Galactic Molecular* H_2

As expected, the largest contaminant of the AGN spectra in the *FUSE* band is absorption by molecular H_2 in our Galaxy. We take this contamination into account by comparing the dips in our observed spectra with simple models of absorption by molecular hydrogen at zero redshift.[2] The H_2 absorption models are characterized by a single component at a kinetic temperature

[1] See http://fuse.pha.jhu.edu/analysis/calfusev31_intro.html.

[2] See http://fuse.pha.jhu.edu/~awf/JBH/.

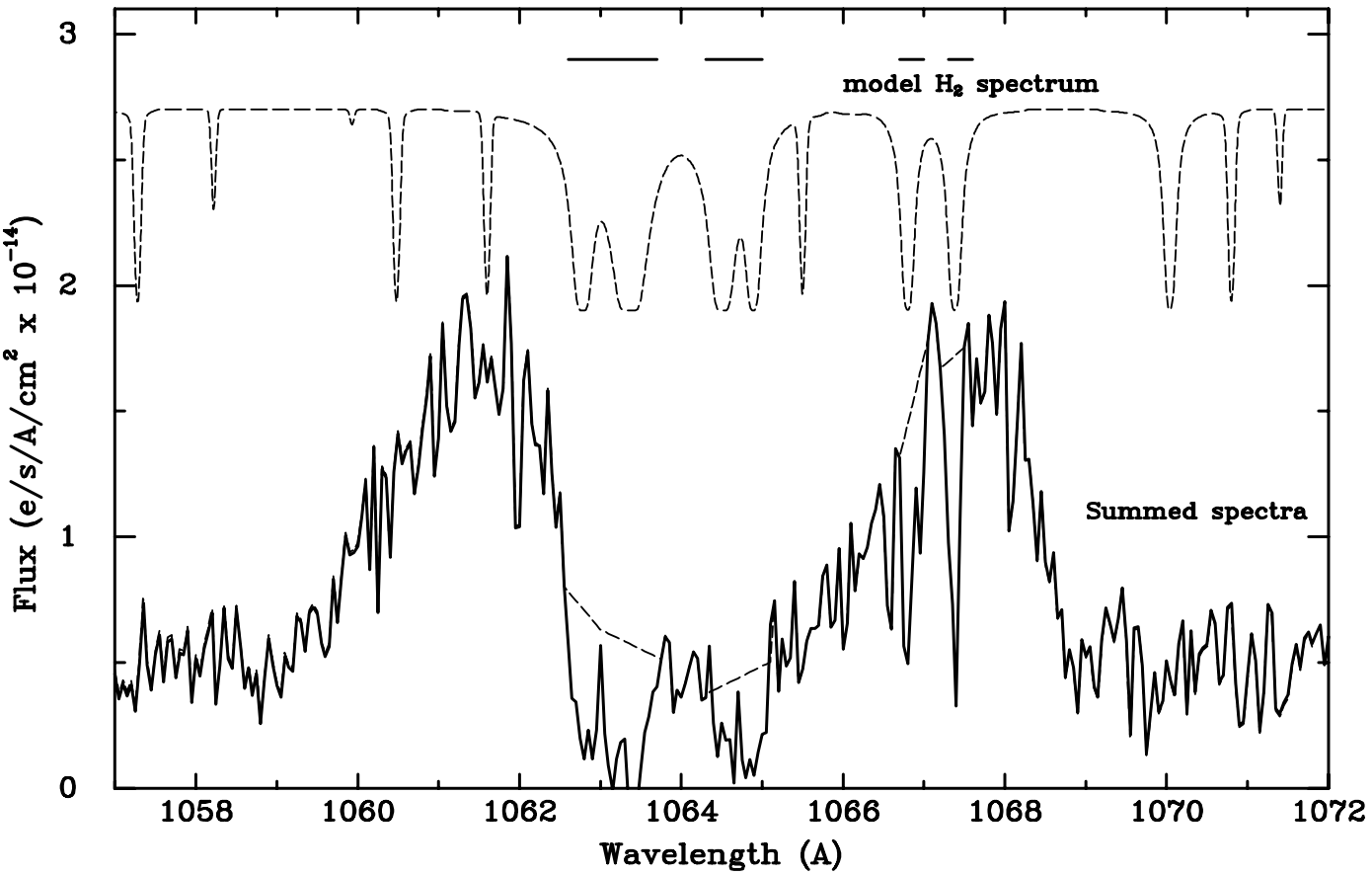

FIG. 1.—The O VI doublet region of the spectrum of Mrk 533. Data from the detectors LiF1A and LiF2B, which give redundant coverage of this region, have been combined (*bottom plot*). The top plot is an example of a model absorption spectrum of Galactic H_2 at zero redshift that corresponds to a H_2 column density of 5×10^{19} cm^{-2} (see § 2.4), showing that several of the dips in the Mrk 533 spectra are contamination from absorption in our Galaxy. The positions of these troughs are indicated by horizontal lines above the upper H_2 spectrum. The dashed lines marked on the O VI spectrum indicate a rough removal of the effects of this absorption (see § 3).

of 300 K, with zero metallicity, the rotational states chosen, a fixed atomic hydrogen column density of 5.0×10^{20} cm^{-2}, and a varying molecular hydrogen column density. More details are discussed in § 3.

2.5. *Reduction of the HST STIS Data*

The *HST* STIS data were calibrated within CalSTIS and cleaned using IRAF `cosmicrays`. The slit location was verified by comparing the integrated flux with Wide Field Planetary Camera 2 (WFPC2) observations taken at similar wavelengths.

We note that the position of the STIS slit along the wavelength axis cannot be determined with the precision we need in order to calibrate the zero point of the wavelength scale. We therefore use the results from the data of Unger et al. (1988) taken with the image dissector scanner (IDS) on the Isaac Newton Telescope for this calibration. In their spectra, the wavelengths of the peak of the [O III] λ5007 emission and of the highly blueshifted component are 5153.0 and 5134.6 Å, respectively, whereas the STIS data with CalSTIS calibration give 5155.4 and 5137.1 Å, respectively, implying an offset between the STIS and ground-based data of +2.4 and +2.5 Å, respectively. We therefore applied a shift of −2.5 Å to the STIS data after calibration with CalSTIS.

3. THE EMISSION LINES IN THE INTRINSIC FAR-UV SPECTRUM OF MRK 533

The only strong line feature detected is the O VI doublet (Fig. 1). The C III emission at 977 Å is seen weakly at its expected redshifted position (Fig. 3). We do not detect the Lyβ λ1026, the He II λ1085, or the Ne III λ991 lines that were seen, e.g., in the Hopkins Ultraviolet Telescope (HUT) spectrum of the archetypal Seyfert 2, NGC 1068 (Kriss et al. 1992). They would have been seen clearly at the equivalent widths observed in NGC 1068, as the continuum signal level in Mrk 533 in those wavelength regions is comparable to that near the O VI doublet.

Also plotted in Figure 1 is a model used for absorption by molecular hydrogen. The corresponding H_2 column density is 5×10^{19} cm^{-2}, although we note that this model is not a unique one corresponding to this column density. An inspection of the dips in the model, and comparison of their widths with the dips in the observed spectra, clearly indicate that there is a correspondence between the strongest H_2 absorptions (marked in Fig. 1) and some of the dips in the observed spectra. The comparison model was chosen by inspection to have widths of the strongest absorptions comparable with those seen in the observed spectrum. The widths of the main absorptions in the region depend significantly on the column density. The data are consistent with the observed dips being due to the strongest H_2 absorptions with a shift of −0.15 Å. This is within the uncertainty in the calibration of the wavelength zero point of the *FUSE* spectrum.

In Figure 2 we show the profiles of the O VI doublet lines in velocity space. There is a small slope to the continuum around the O VI lines in the range 1050–1075 Å that rises with wavelength (Fig. 1). This slope is likely to be real and is also present in the archival spectrum that uses the *FUSE* pipeline background subtraction. We discuss possible extinction effects later. As we

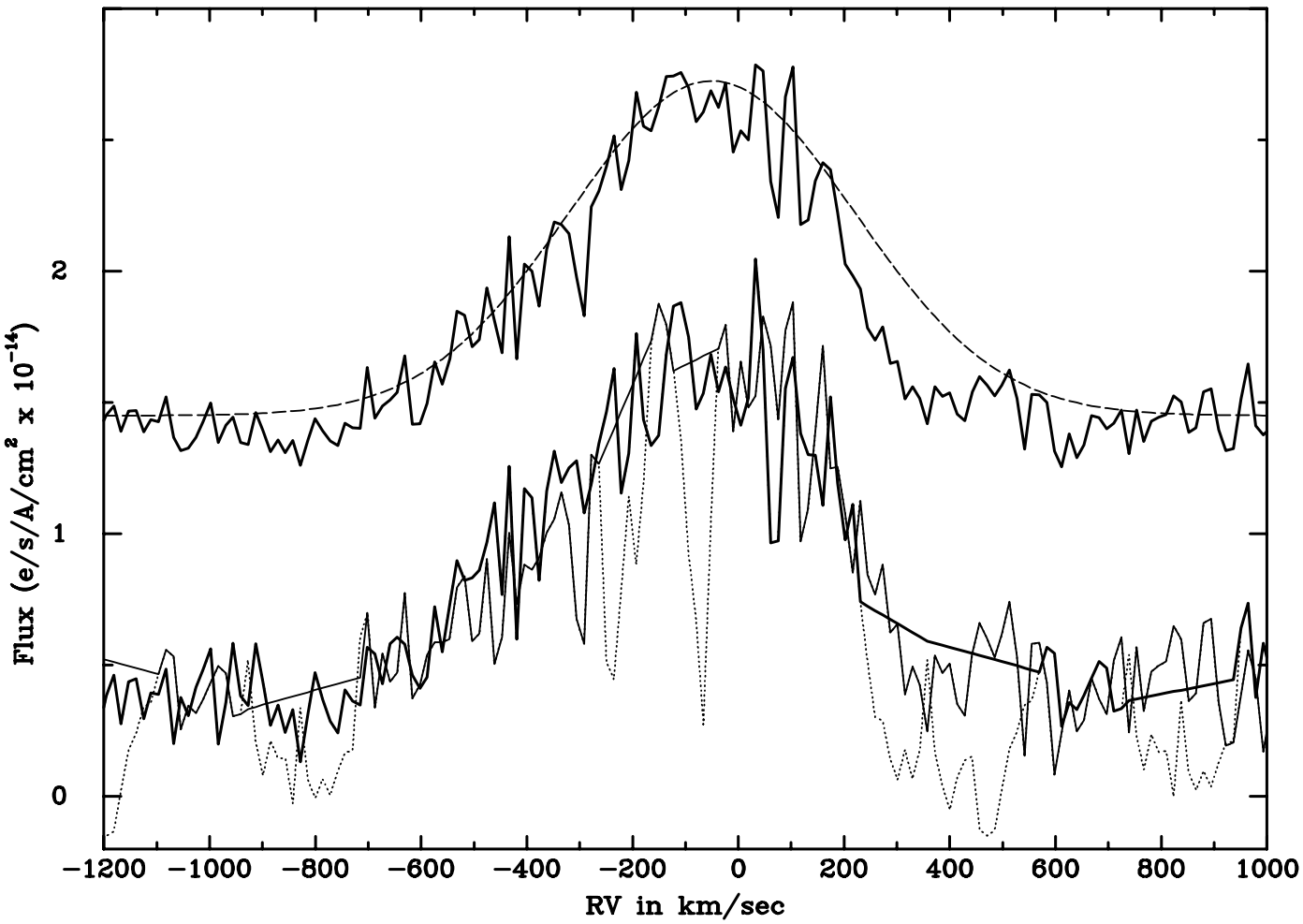

FIG. 2.—Mrk 533 spectra in the O VI region plotted in velocity space. A systemic redshift of 0.02888 (heliocentric velocity of 8659 km s^{-1}) and a doublet separation of 5.85 Å has been assumed. In the lower plot, the heavy and light solid lines represent the spectra of the 1032 and 1038 Å lines, respectively. The dotted lines represent the dips in these spectra that are assumed to be due to H_2 absorption, and the corresponding solid lines show their rough removal (see § 3 for further details). The averaged profile is plotted in the top plot along with a symmetrical (Gaussian) profile for comparison, which illustrates the shortward asymmetry of the observed profiles, as well as the suggestive residual absorption troughs at ~ -300 and -800 km s^{-1}. If real, these troughs could be intrinsic to Mrk 533.

are concerned here with the emission-line profiles, in plotting Figure 2 we have simply subtracted the slope in the continuum across the O VI emission lines, by subtracting a linear continuum using the points at 1057–1058 Å and 1071–1073 Å. The diagrams show a level continuum at 4×10^{-15} ergs cm^{-2} s^{-1} $Å^{-1}$.

The heliocentric systemic velocity of 8659 km s^{-1} (see 5.2) was adopted for the velocity zero of the plot. The shift between the profiles of 5.85 Å is the separation of the O VI doublet redshifted by 0.02888. Apart from the removal of the linear slope, no other scaling was done.

Clearly, the two profiles match within the noise except for a few troughs that in fact correspond to those in the illustrated H_2 absorption model. We show in Figure 2 the result of a rough removal of this assumed contamination, estimated by comparing with the model H_2 spectrum. The heavy solid and light solid curves represent the 1032 and 1038 Å lines, respectively. All the dips in each of the observed profiles that are assumed to be due to contaminating Galactic H_2 absorption are shown as a dotted line. In the case of each removal, the straight line compares well with the profile of the other line in that velocity region within the noise. The removals are also indicated in Figure 1.

Given the good match of the profiles of the O VI doublet, they were combined to form a mean, plotted in Figure 2. The profiles show an asymmetry about zero velocity in the form of an extension toward shorter wavelengths. Two possible dips remain in the average profile, corresponding to velocities of -300 and -800 km s^{-1}.

The spectrum of the C III λ977 line (see Fig. 3) is rather noisy, and apart from its detection, no definitive statement can be made about its profile. While it is interesting that data from both the LiF channels show a relatively deep dip in a region that is clear of any H_2 absorption and corresponds to a velocity of ~ -200 km s^{-1}, we consider this to be of only marginal significance in view of the low S/N.

4. THE [O III] λ5007 VELOCITY STRUCTURE OF MRK 533 FROM *HST* STIS

In Figure 4, the *HST* STIS spectral image in the rest-frame [O III] λ5007 spectral region is plotted in velocity space. The vertical axis is in the direction of the STIS slit, which was oriented parallel to the radio axis (P.A. = 124°). The spatial zero point on this axis is the nominal nuclear position, taken to be the peak in the continuum. (It is possible that the true nucleus is shifted with respect to this position, since the obscuring dust in the line of sight would be expected to attenuate its emission, thereby effectively shifting the continuum peak.) The zero position on the

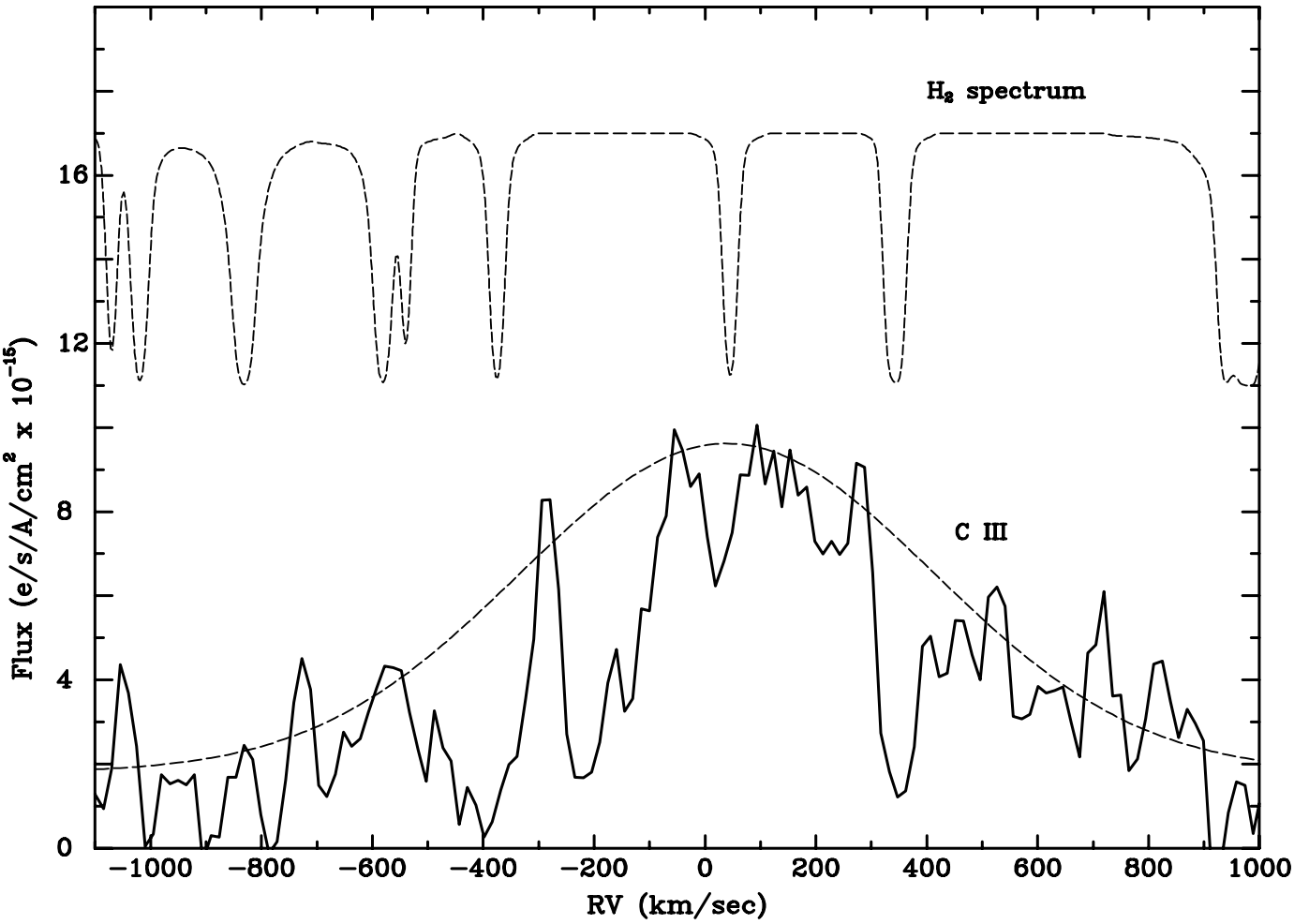

FIG. 3.—Spectrum in the C III region plotted in velocity space. The S/N is much lower in this region, but nevertheless the C III emission is detected. The model H_2 absorption spectrum at zero redshift is plotted on top. A symmetrical (Gaussian) profile is plotted to guide the eye, but no attempt has been made to remove the effect of Galactic H_2 absorption. A trough is seen (in both detectors, combined here) in a region that is clear of Galactic H_2 absorption, which corresponds to a velocity of -200 km s^{-1}, but is at best of marginal significance.

horizontal dispersion axis corresponds to the heliocentric systemic velocity.

Clearly, the [O III] λ5007 emission is spatially asymmetric, with most of the emission to the northwest of the nominal nuclear position, along the radio axis (see images in Unger et al. 1988; Momjian et al. 2003). On the continuum peak, the [O III] λ5007 profile peaks close to the systemic velocity and has a "blue shoulder" at ~ -100 km s^{-1} (similar to what was reported earlier by Unger et al. 1988; Veilleux 1991b). Roughly 0.″1 to the northwest, the peak shifts to $\sim +200$ km s^{-1}, while there is a broad blueshifted peak at ~ -1000 km s^{-1} with an extended wing reaching ~ -2000 km s^{-1}. The spatial extent of this broad maximum appears to be 0–0.″2.

5. DISCUSSION

We assume in our analysis that all the spectral emission in the *FUSE* data is attributable to the AGN and its photoionization effects, and that even in the $30'' \times 30''$ aperture, the contribution from hot stars is negligible. This assumption is supported by a comparison of the Mrk 533 spectrum with the *FUSE* spectra from hot stars in the atlas of Walborn et al. (2002). None of the expected strong emission lines from stars is seen in our spectra, so we assume that all emission arises in the AGN.

We also recall that in, e.g., NGC 3516, Hutchings et al. (2001) found from a comparison of contemporaneous large-aperture *FUSE* spectra and narrower aperture *HST* STIS spectra that the continuum levels in the overlapping spectral region match very well. They conclude, therefore, albeit for a Seyfert 1, that the continuum is dominated by nuclear emission and there is no significant contribution to the *FUSE* photons from starlight at larger radii.

5.1. *The Line Ratio of the* O VI *Doublet*

The statistical weights of the upper levels of the O VI doublet transitions are two and four for the longward and shortward wavelength lines, respectively, implying an intensity ratio of 2 for the doublet, under the assumptions that the emission is optically thin and that the emitters are in local thermodynamic equilibrium (LTE; Mauche & Raymond 1998). In the Seyfert 1 galaxies, this is indeed the typical ratio that has been found for the broad emission-line region (G. A. Kriss 2005, private communication).

In Mrk 533, however, the two doublet lines of the O VI emission match very well in both intensity and profile, as can be seen from Figure 2. We estimate the line flux in both cases to be $\sim(3.7 \pm 0.2) \times 10^{-14}$ ergs s^{-1} cm^{-2}. Thus, the doublet ratio is $\sim$1, similar to the value inferred from HUT data for NGC 1068 by Kriss et al. (1992) and in contrast to the trend seen in Seyfert 1 galaxies. This means that the O VI line is optically thick over roughly the whole velocity range in Mrk 533. These aspects are

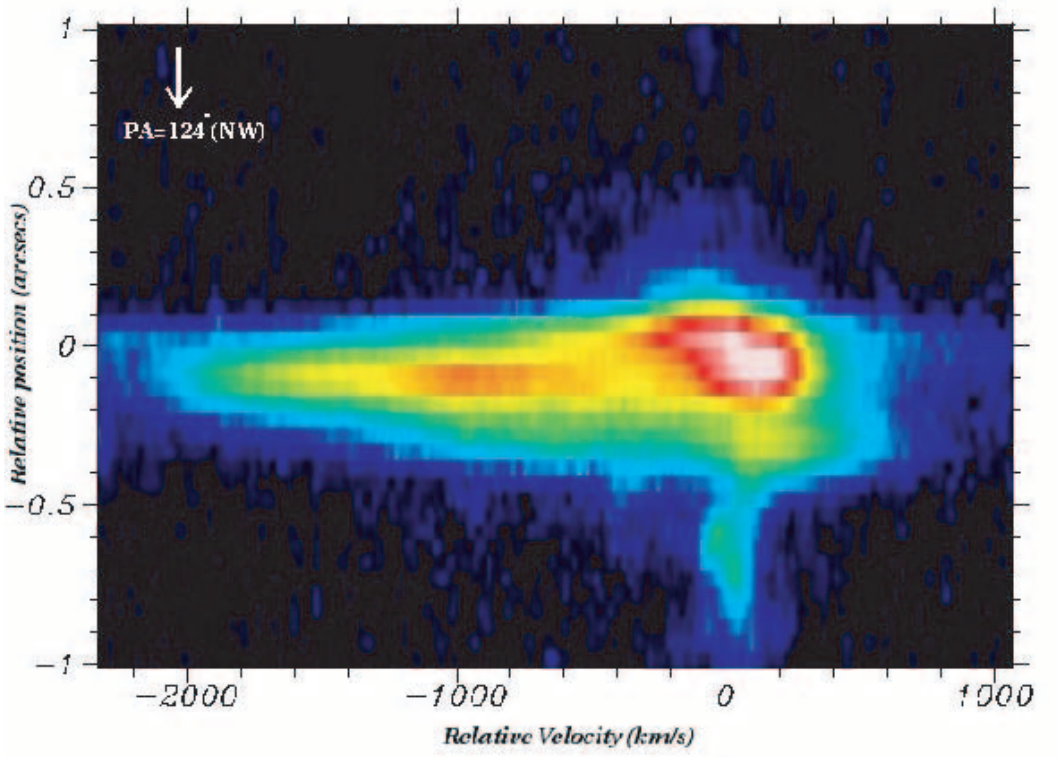

FIG. 4.—*HST* STIS spectral image of Mrk 533 in the region of the [O III] λ5007 line, plotted in velocity space. The vertical spatial axis is along the STIS slit at a P.A. of 124° (along the radio axis). The zero position of this axis corresponds to the peak of the continuum in the off-line region. The zero position of the horizontal dispersion axis corresponds to the systemic velocity of 8659 km s^{-1} (see § 4).

being investigated in detail in a subsequent paper (P. Shastri et al. 2006, in preparation).

We note that the effect of the rising slope of the continuum in the wavelength range 1055–1075 Å (see § 3) has been taken out in plotting Figure 2, and thus it clearly does not alter our conclusion about the line ratio of the doublet.

5.2. *Shifts of the Lines Relative to Systemic*

We use a heliocentric systemic velocity $cz = 8659$ km s^{-1}, which is the mean of the host galaxy stellar velocity from Nelson & Whittle (1995) and the values derived by Unger et al. (1988) and Nishiura et al. (2000) from their Hα rotation curves. The corresponding heliocentric redshift is 0.02888.

Within the spectral resolution constraint of the *FUSE* data, the recession velocities derived from the peaks of the O VI doublet and the C III line are consistent with the systemic velocity. Right at the nominal nuclear position, the [O III] λ5007 peak is also at systemic (Fig. 4), although a larger aperture would find the strongest near-nuclear [O III] λ5007 emission to be redshifted by $\sim$200 km s^{-1}. This shift relative to systemic was noted from ground-based spectra by Unger et al. (1988; [O III] λ5007) and Nelson & Whittle (1995; [S III] λ9069). It is likely that such spatial and velocity structure accounts for other small redshift differences noted in the literature, such as the peak Hα of 8756 km s^{-1} measured by Veilleux (1991a). Two other velocities deserve mention. The CO emission is centered essentially at systemic (8669 km s^{-1}; Sanders & Mirabel 1985), as one might expect for dense gas relatively deep in the galaxy potential. Finally, H I is seen in slightly blueshifted absorption (8623 km s^{-1}; Beswick et al. 2002), consistent with a modest outflow on $\sim$100 pc scales. Tidal interactions with the other galaxies of the compact group (Verdes-Montenegro et al. 1997) can also create shifts in the overall peak of the neutral gas.

5.3. *Intrinsic Absorption by Molecular Hydrogen*

We do not find any H_2 absorption that is intrinsic to Mrk 533 (e.g., from the putative torus, given that it is a Seyfert 2). Indeed, since the nuclear continuum emission is expected to be attenuated due to obscuration, it is not surprising that it is too weak to measure any absorption against it.

5.4. *Absorption in the Outflow?*

Strong absorptions in the profile of the FUV emission lines are a characteristic feature of the Seyfert 1 galaxies observed by *FUSE* (e.g., Kriss 2006). In the case of Mrk 533, however, the evidence for absorption is less definitive. This is not entirely surprising for a Seyfert 2, given that the nuclear continuum is expected to be significantly attenuated and that the outflow is expected to be primarily along the AGN axis and obscured in the near-nuclear region.

The combined profile in Figure 2 shows two dips in both lines of the O VI doublet, at -300 and -800 km s^{-1} (see Fig. 2). These are residual dips that remain after accounting for absorption by Galactic H_2 and have no local identification. Their significance is not high, however, and better S/N data are required for any definitive interpretation. If real, they would have to be due to absorbers intrinsic to Mrk 533: it is possible that the absorption at -300 km s^{-1} is associated with the outflow from the nucleus, but could also be from an interstellar cloud associated with the circumnuclear starburst that is known to be present in Mrk 533. The latter absorption (at -800 km s^{-1}), on the other hand, has too large a velocity to be associated with such a starburst, which

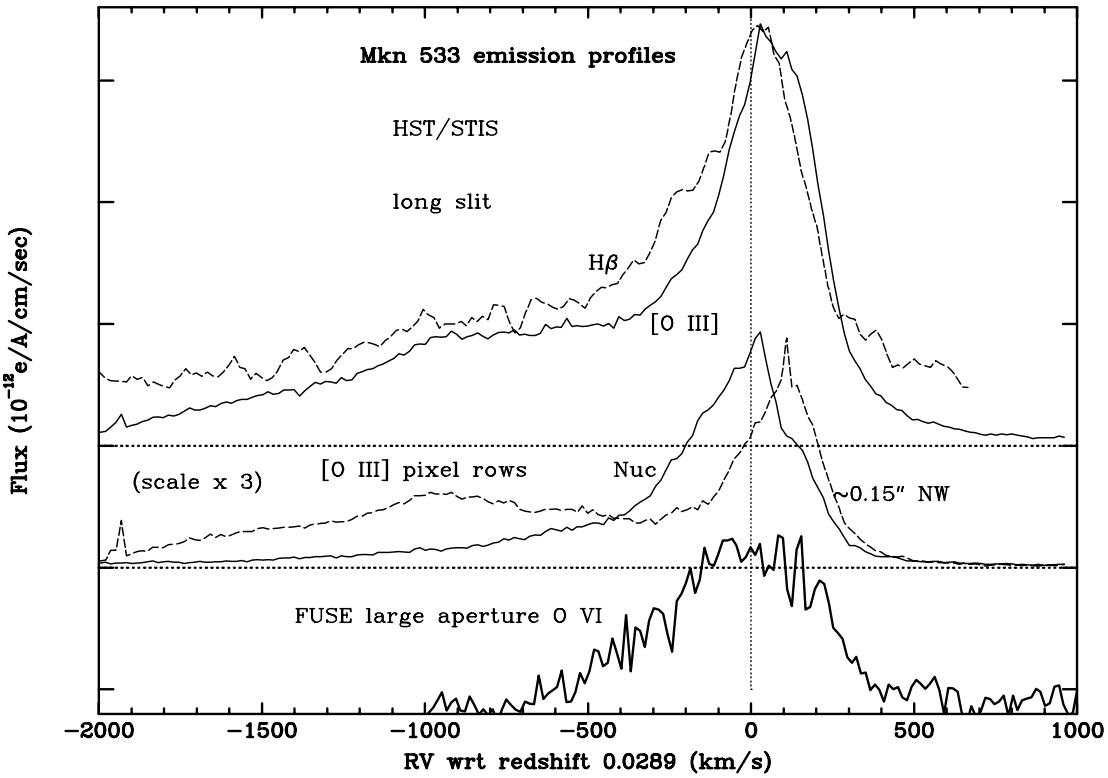

FIG. 5.—Profiles of the [O III] λ5007 and Hβ lines from the *HST* STIS data, plotted together with the O VI profile from *FUSE*. In the top plot, the solid and dashed curves represent the profiles of the [O III] λ5007 and Hβ lines, respectively, as extracted from a STIS long-slit aperture. In the middle plot, the solid curve represents the profile of the [O III] λ5007 line extracted from a "nuclear" aperture (the 42nd pixel row in the STIS data that is at the continuum position). The dashed curve represents the profile from the off-nuclear region, $\sim$0.″15 northwest from the "nucleus" (pixel row 39). The *y*-scale in this plot is magnified by a factor of 3. The solid curve in the bottom plot is the O VI profile from the *FUSE* spectrum from Fig. 2, to compare and contrast with the STIS profile.

would imply that it would have to be due to a foreground cloud associated with the outflow.

In the case of the C III emission line, our data are very noisy, and although there is a suggestion of a dip in both the photon channels in a region clear of any Galactic H_2 absorption that corresponds to a velocity of -200 km s^{-1}, this feature is at best of marginal significance.

5.5. *The Line Profiles and Their Blueward Asymmetry*

The fact that the O VI emission lines are narrow (e.g., comparable to the width of the core of the [O III] λ5007 line; see Fig. 5) is, of course, consistent with the basic classification of Mrk 553 as a Seyfert 2. In Seyfert 1 galaxies, the O VI lines are usually much broader, although some have an additional narrow component (Kriss 2004).

Figure 5 compares the O VI and [O III] λ5007 emission profiles. The STIS profiles in this plot were extracted using (1) a "nuclear" aperture corresponding to one pixel row centered on the zero position; (2) an "off-nuclear" aperture corresponding to a pixel row $\sim$0.″15 to the northwest, relative to the zero position; and (3) the whole long-slit aperture. The combined profile of the two O VI doublet lines is also shown.

It has long been known that Mrk 533 has a spectacular blue wing to its [O III] λ5007, Hβ, and Hα profiles, and a less striking wing in the N II profile (e.g., Afanasev et al. 1980; Unger et al. 1988; Veilleux 1991a). A striking feature of the *FUSE* profile of the O VI doublet is that it also shows an asymmetry in the same sense. However, it lacks the extended wing shortward of the peak wavelength seen in the lower ionization lines to -2000 km s^{-1}, and its peak also appears centered near the systemic velocity, unlike the long-slit (large-aperture) [O III] λ5007 profile (Fig. 5, *top plot*). Previously, de Robertis & Shaw (1990) had shown that the asymmetry of the emission lines correlates with the ionization potential, for several Seyferts including Mrk 533, but its O VI line clearly does not fit this correlation.

Before concluding that the differences between the profiles of the [O III] λ5007 and O VI lines are real, we must consider the impact of different aperture sizes on the profile shapes. In fact, the large size of the *FUSE* aperture introduces two potential concerns. The first is that extended O VI emission might be included. However, the low excitation measured outside the nucleus (e.g., [O III]/H$_\beta$ < 0.5; Unger et al. 1988) suggests that there will be little if any off-nuclear O VI contribution. Second, mis-centering the Mrk 533 nucleus in the aperture could lead to significant wavelength uncertainty. In our case, however, we used the values from the LiF1A (guiding) channel, which guarantees good centering, and we have determined that the uncertainty is $\leq$45 km s^{-1} (see § 2.1). Hence, we conclude that the peak of the O VI emission is indeed centered on systemic within the errors, and that it indeed lacks the very extended wing shortward of the peak that is seen in the total [O III] λ5007 profile. This is in fact consistent with the O VI emission arising within 0.″05 of the nucleus, since this matches the narrower [O III] λ5007 profile from this innermost region (see Fig. 5). Thus, although the long-slit aperture of the [O III] λ5007 STIS observation (Fig. 5, *top plot*) resembles most closely the *FUSE* aperture in spatial scale, nevertheless the O VI profile actually closely resembles—in both shape and position with respect to systemic—the *nuclear* [O III] λ5007 profile, which we know arises within $\sim$ 0.″05 or $\sim$30 pc from the continuum source. This suggests that the O VI emission arises from this inner $\sim$0.″05 region, similar to what has been conjectured for the narrow component to the O VI line in, e.g.,

NGC 3516 (Hutchings et al. 2001). We also note that the similarity of the O VI and the nuclear [O III] λ5007 profiles argue against complex extinction in this region.

Clearly, beyond 0.″05 or ~30 pc from the continuum peak (and by implication, beyond at least this distance from the putative nucleus), the [O III] λ5007 profile is dominated by the blue wing. If there is corresponding redshifted emission from a receding part of the outflow, it must be hidden from view.

Of relevance here is the fact that the low-ionization lines of Mrk 533 (Veilleux 1991a) do show the extended blue wings up to ~ -2000 km s^{-1}. The case of Hβ from our data is shown in Figure 5. An archival *HST* Faint Object Spectrograph (FOS) spectrum shows that the Mg II λ2798 line has a similar profile.

In this picture, the ionization parameter drops sufficiently quickly with distance from the nucleus so that the O VI line is no longer generated in the blue wing gas found ~0.″1–0.″2 (50–100 pc) off nucleus. This off-nuclear gas, it would seem, has been accelerated by either a nuclear wind or the near-nuclear radio-emitting hot spot (seen, e.g., in the images of Momjian et al. [2003], which exhibit structures in approximately the same location). Evidence for accelerated flows on scales of 0.″2 has been found in several Seyferts by Ruiz et al. (2005). It is perhaps relevant here that there is also direct evidence for acceleration in some Seyfert 1 galaxies (e.g., Hutchings et al. 2001; de Kool 1997), although on a somewhat smaller physical scale.

The blue wing is most commonly interpreted as arising from outflow of line-emitting gas with a distributed source of opacity (dust) that obscures the far side (e.g., Whittle 1985; Veilleux 1991b). The alternative—infalling dusty clouds emitting preferentially from the side facing the central source—seems unlikely in this case, not least because some of the highest velocity blueshifted gas is seen off nucleus where we know the gravitational velocities are a factor of 10 smaller. Figure 4 shows that most of the [O III] λ5007 emission comes from a region northwest of the nucleus, which reinforces the idea that the [O III] λ5007 emission arises from an approaching outflow, the receding side of which is hidden. The torus in the line of sight could provide the opacity required to produce the blue wings, by obscuring the photons from the redshifted part of the profile, which would be those closest to the nucleus but moving away from us. It perhaps also contributes significantly to the obscuration of the [O III] λ5007 emission from the southeast side of the nuclear region, making the [O III] λ5007 structure appear one-sided. It may be recalled that the host galaxy of Mrk 533 is oriented face-on, an unexceptional fact, given the lack of correlation between the host galaxy axis and the AGN axis in Seyferts (Schmitt et al. 2003).

Thus, if the "shoulders" shortward of the peak in both the [O III] λ5007 and O VI profiles originate in the same gas, it means that the shortward asymmetry of the O VI emission results from a high excitation outflow within 0.″05 or ~30 pc from the nucleus, and any corresponding redshifted emission from the receding part of the outflow is hidden from view.

Obscuration of the receding flow implies that dust is present and may affect what we see of the approaching flow too. The small rise in the continuum with wavelength implies some extinction of the nuclear continuum. The redshifted peak of the [O III] λ5007 line relative to systemic 0.″15 northwest of the nucleus could be understood in this picture. Kraemer et al. (1994) quoted a reddening value $E(B-V) = 0.20$ based on the line flux ratios, but given the uncertainties in the extinction curve in the *FUSE* range, we are unable to quantitatively comment on the consistency of our continuum slope with this reddening value. Using our line fluxes for the O VI, and the Hβ line flux from Kraemer et al. (1994), the line ratio of O VI/Hβ is ~0.6. Patchy dust could of course complicate all the profiles, and we would need much more detailed evidence to consider that. For now, we note particularly that the O VI profile is very similar to the nuclear [O III] profile. However, given the significant differences in the overall shapes of the O VI and off-nuclear [O III] λ5007 profiles even in regions where the S/N is high, it is very unlikely that such differences can arise from dust extinction and therefore must be principally attributed to velocity and ionization gradients.

A further conclusion from the absence of an extended shortward wing in the O VI profile is that this high-velocity gas is likely to be *photoionized* by the central source, rather than *shock ionized* by a wind or jet. In the shock-ionization picture, one would expect, at least naively, that the highest velocity gas would have the highest ionization. That this is not the case in Mrk 533 argues against shock ionization. A more detailed analysis using lower ionization lines gave a similar result for Mrk 78 (Whittle et al. 2005), but in the case of Mrk 533 the large difference in the degree of ionization between O^{5+} and O^{2+} makes for a stronger case.

Finally, we note that the picture described here is also consistent with the spectropolarimetric results of Tran (1995), who found that the [O III] λ5007 profile in polarized light was narrower and had no extended blue wing. The region producing the scattered light is likely to be highly nuclear (after all, the polarized spectrum shows broad Hβ), and hence it is not surprising that the scattered [O III] λ5007 profile matches our most nuclear STIS data: narrower profile, centered on systemic, and with little blue wing—indeed similar to the O VI profile.

If the outflow is in the form of a hollow bicone (e.g., Ruiz et al. 2005), then, depending on the opening angle and the inclination of the line of sight, we may see both approaching and receding velocities along the line of sight from the approaching "cone." The obscuring torus may then also affect the nuclear part of the emission profile from the approaching cone and, e.g., preferentially obscure the approaching velocities. The redshifted peak of the [O III] λ5007 line relative to systemic could be understood in this picture, although we do not have enough spatial resolution to model it in detail.

6. CONCLUSIONS

We present high-resolution *FUSE* spectra of the permitted ultraviolet O VI $\lambda\lambda$1032, 1038 and C III λ977 lines, and *HST* STIS spectra of the [O III] λ5007 optical line, of the Seyfert 2 galaxy Mrk 533 (NGC 7674). We find the following:

1. The O VI doublet lines are strong and relatively narrow, consistent with their origin in the narrow-line region. This is in predicted contrast to the very broad O VI line reported in Seyferts of type 1 that are purportedly pole-on.

2. The C III λ977 emission line is also weakly detected with similar line width, but the Lyβ λ1026, He II λ1085, and Ne III λ991 emission lines are not detected.

3. The profiles of the two doublet lines of O VI emission are very well matched, implying a line ratio of ~1 and thus optically thick emission. This fact is also consistent with the O VI doublet not originating in a broad-line region, which typically shows a flux ratio ~2.

4. After correcting for Galactic H_2 absorption, we identify with somewhat marginal significance two possible intrinsic absorption features in the O VI profile at -300 and -800 km s^{-1}.

5. The O VI velocity profile is centered near the systemic velocity and has a moderate shortward asymmetry. This matches quite well the [O III] λ5007 profile from the innermost pixel (<0.″05; i.e., <30 pc) of the STIS data.

6. However, moving only slightly off nucleus (0.″1–0.″2, or 50–100 pc), the [O III] λ5007 profile peak shifts to +100 km s^{-1}, and the shortward side gains a strong wing extending to $\sim$−2000 km s^{-1}.

7. The difference between the O VI and [O III] λ5007 profiles is consistent with a picture in which the most nuclear region exhibits velocities $\sim$500 km s^{-1} in mild outflow with the receding part hidden from view. However, beyond this inner region, the gas is strongly accelerated by a nuclear wind or jet flow. The narrow and symmetric profile of the polarized [O III] λ5007 line is also consistent with this picture.

8. The absence of O VI emission in the highly accelerated [O III] λ5007 emitting gas argues in support of this gas being photoionized rather than shock ionized.

Help from the *FUSE* team during the proposal and observation stages, and the efforts that have gone into the high quality of their user services, are gratefully acknowledged. We thank Suzy Collin for several insightful discussions, and the anonymous referee whose comments improved the paper very significantly. This paper is based on observations made with the NASA-CNES-CSA *Far Ultraviolet Spectroscopic Explorer*. *FUSE* is operated for NASA by the Johns Hopkins University, under NASA contract NAS5-32985. The *HST* STIS spectra are based on observations obtained at the Space Telescope Science Institute, which is operated by the Association of Universities for Research in Astronomy, Inc., under NASA contract NAS5-26555. Support for the *HST* proposal GO-8453 was provided by NASA through a grant from the Space Telescope Science Institute. The *FUSE* research was supported by NASA grant NAG5-13726. This research has made use of the Canadian Astronomy Data Centre (CADC), NASA's Astrophysics Data System bibliographic services, and the NASA/IPAC Extragalactic Database (NED), which is operated by the Jet Propulsion Laboratory, California Institute of Technology, under contract with NASA.

REFERENCES

Afanasev, V. L., Lipovetskii, V. A., Markarian, B. E., & Stepanian, D. A. 1980, Astrofizika, 16, 193
Antonucci, R. 1993, ARA&A, 31, 473
Antonucci, R. R. J., & Miller, J. S. 1985, ApJ, 297, 621
Beswick, R. J., Pedlar, A., & McDonald, A. R. 2002, MNRAS, 335, 1091
Curran, S. J., Polatidis, A. G., Aalto, S., & Booth, R. S. 2001, A&A, 373, 459
de Kool, M. 1997, in ASP Conf. Ser. 128, Mass Ejection from Active Galactic Nuclei, ed. N. Arav, I. Shlosman, & R. J. Weymann (San Francisco: ASP), 233
de Robertis, M. M., & Shaw, R. A. 1990, ApJ, 348, 421
de Vaucouleurs, G., de Vaucouleurs, A., Corwin, H. G., Buta, R. J., Paturel, G., & Fouque, P. 1995, Third Reference Catalogue of Bright Galaxies (Berlin: Springer) (RC3)
Dultzin-Hacyan, D., Krongold, Y., Fuentes-Guridi, I., & Marziani, P. 1999, ApJ, 513, L111
Elvis, M., Maccacaro, T., Wilson, A. S., Ward, M. J., Penston, M. V., Fosbury, R. A. E., & Perola, G. C. 1978, MNRAS, 183, 129
Hutchings, J. B., Kriss, G. A., Green, R. F., Brotherton, M., Kaiser, M. E., Koratkar, A. P., & Zheng, W. 2001, ApJ, 559, 173
Kinney, A. L., Antonucci, R. R. J., Ward, M. J., Wilson, A. S., & Whittle, M. 1991, ApJ, 377, 100
Kraemer, S. B., Wu, C., Crenshaw, D. M., & Harrington, J. P. 1994, ApJ, 435, 171
Kriss, G. A. 2004, in IAU Symp. 222, The Interplay among Black Holes, Stars and ISM in Galactic Nuclei, ed. T. Storchi Bergmann, L. C. Ho, & H. R. Schmitt (Cambridge: Cambridge Univ. Press), 223
———. 2006, in ASP Conf. Proc. 348, Astrophysics in the Far Ultraviolet, ed. G. Sonneborn, H. W. Moos, & B.-G. Andersson (San Francisco: ASP), 499
Kriss, G. A., Davidsen, A. F., Blair, W. P., Ferguson, H. C., & Long, K. S. 1992, ApJ, 394, L37
Malaguti, G., et al. 1998, A&A, 331, 519
Malkan, M. A., Gorjian, V., & Tam, R. 1998, ApJS, 117, 25
Mauche, C. W., & Raymond, J. C. 1998, ApJ, 505, 869
Miller, J. S., & Goodrich, R. W. 1990, ApJ, 355, 456
Momjian, E., Romney, J. D., Carilli, C. L., & Troland, T. H. 2003, ApJ, 597, 809
Moos, H. W., et al. 2000, ApJ, 538, L1
Moran, E. C., Barth, A. J., Kay, L. E., & Filippenko, A. V. 2000, ApJ, 540, L73
Murthy, J., & Sahnow, D. J. 2004, ApJ, 615, 315
Nelson, C. H., & Whittle, M. 1995, ApJS, 99, 67
Nishiura, S., Shimada, M., Ohyama, Y., Murayama, T., & Taniguchi, Y. 2000, AJ, 120, 1691
Osterbrock, D. E. 1989, Astrophysics of Gaseous Nebulae and Active Galactic Nuclei (Mill Valley: Univ. Science Books)
Pogge, R. W., & Martini, P. 2002, ApJ, 569, 624
Ruiz, J. R., Crenshaw, D. M., Kraemer, S. B., Bower, G. A., Gull, T. R., Hutchings, J. B., Kaiser, M. E., & Weistrop, D. 2005, AJ, 129, 73
Sahnow, D. J., et al. 2000, Proc. SPIE, 4139, 131
Sanders, D. B., & Mirabel, I. F. 1985, ApJ, 298, L31
Schmidt, M., & Green, R. F. 1983, ApJ, 269, 352
Schmitt, H. R., Donley, J. L., Antonucci, R. R. J., Hutchings, J. B., Kinney, A. L., & Pringle, J. E. 2003, ApJ, 597, 768
Tran, H. D. 1995, ApJ, 440, 578
Unger, S. W., et al. 1988, MNRAS, 234, 745
Veilleux, S. 1991a, ApJS, 75, 357
———. 1991b, ApJ, 369, 331
Veilleux, S., Goodrich, R. W., & Hill, G. J. 1997, ApJ, 477, 631
Verdes-Montenegro, L., del Olmo, A., Perea, J., Athanassoula, E., Marquez, I., & Augarde, R. 1997, A&A, 321, 409
Walborn, N. R., Fullerton, A. W., Crowther, P. A., Bianchi, L., Hutchings, J. B., Pellerin, A., Sonneborn, G., & Willis, A. J. 2002, ApJS, 141, 443
Whittle, M. 1985, MNRAS, 213, 1
Whittle, M., Rosario, D. J., Silverman, J. D., Nelson, C. H., & Wilson, A. S. 2005, AJ, 129, 104